First-principles study on the material properties of the inorganic perovskite $Rb_{1-x}Cs_xPbI_3$ for solar cell applications

Un-Gi Jong,[1,2] Chol-Jun Yu,[1,*] Yun-Sim Kim,[1] Yun-Hyok Kye,[1] and Chol-Ho Kim[2]

[1]*Department of Computational Materials Design, Faculty of Materials Science, Kim Il Sung University, Ryongnam-Dong, Taesong District, Pyongyang, Democratic People's Republic of Korea*

[2]*Natural Science Centre, Kim Il Sung University, Ryongnam-Dong, Taesong District, Pyongyang, Democratic People's Republic of Korea*

(Received 12 June 2018; published 10 September 2018)

Recently, replacing or mixing organic molecules in hybrid halide perovskites with inorganic Cs or Rb cations was reported to increase the material stability with comparable solar cell performance. In this work, we systematically investigate the electronic and optical properties of all-inorganic alkali iodide perovskites $Rb_{1-x}Cs_xPbI_3$ using first-principles virtual-crystal approximation calculations. Our calculations show that with increasing the Cs content x, band gaps, exciton binding energies, and effective masses of charge carriers decrease following the quadratic (linear for effective masses) functions, while lattice constants and static dielectric constants increase following the quadratic function, indicating an enhancement of solar cell performance upon the Rb addition to $CsPbI_3$. By including the many-body interaction within the GW approximation and incorporating the spin-orbit coupling (SOC), we obtain a more reliable band gap compared with experiment for $CsPbI_3$, highlighting the importance of using the GW+SOC approach for the all-inorganic and organic-inorganic hybrid halide perovskite materials.

DOI: 10.1103/PhysRevB.98.125116

I. INTRODUCTION

Recently, perovskite solar cells (PSCs) have emerged as the most promising photovoltaic (PV) solar cells due to the low cost of raw materials, ease of the manufacturing process [1,2], and, moreover, rapidly evolving power conversion efficiency (PCE) over 22% [3]. In general, PSCs include the organic-inorganic halide perovskite as the major component, with a chemical formula ABX_3, where A is an organic monovalent cation like methylammonium ($MA = CH_3NH_3$) or formamidinium [$FA = HC(NH_2)_2$], B is an inorganic divalent cation (Pb or Sn), and X is a halogen anion (I, Br, Cl). As a typical example, $MAPbI_3$ possesses many good properties for a solar absorber [4], such as appropriate band gaps for light absorption [5], low exciton binding energy [6], high charge carrier mobilities [7], and tolerable defect properties [8]. However, its poor material stability, especially under heat and humidity conditions, imposes restrictions on the long-term stability of PSCs, which is the most challenging obstacle to the large-scale commercial application of PSCs [9,10]. In the organic-inorganic hybrid perovskites, the organic molecules such as MA and FA are particularly sensitive to moisture and/or oxygen due to their high hygroscopicity, and thus, it is not easy to prevent their decomposition, leading to the degradation of PSCs upon exposure to moisture.

To resolve this issue, replacing the organic cations MA and FA with inorganic monovalent alkali cations such as cesium and rubidium has been suggested as a favorable way due to their lower sensitivity to moisture [11,12]. Although the Cs^+ (1.67 Å) and Rb^+ (1.52 Å) cations have a smaller ionic radius than MA^+ (1.80 Å) or FA^+ (1.90 Å), their Goldschmidt tolerance factors for $APbI_3$ perovskites, defined as $\alpha = (r_A + r_X)/\sqrt{2}(r_B + r_X)$ with ionic radii r, are 0.81 and 0.78 [13], within the proper range $0.7 < \alpha < 1$ for stable halide perovskites [14–16]. In fact, all-inorganic cesium lead iodide perovskite ($CsPbI_3$) has been reported to significantly increase device stability with PV performance comparable to that of the organic-inorganic hybrid PSCs [17–19]. Actually, the smaller ionic radius of the Cs^+ cation, compared with the MA^+ cation, leads to an octahedral tilting and, accordingly, a widening of the band gap E_g from 1.50 eV in $MAPbI_3$ [5] to 1.73 eV in $CsPbI_3$ with a cubic phase [20], which is within the optimum range $1.7 < E_g < 1.8$ eV for a top cell material in tandem with a crystalline Si bottom cell [21]. It should be noted that other cesium halide perovskites such as $CsPbBr_3$ and $CsPbI_3$ have much higher band gaps of 2.3 and 3.0 eV, respectively [18,22]. Keeping in mind that crystalline $CsPbI_3$ has two phases, i.e., the photoactive black phase with a cubic lattice (α-$CsPbI_3$) at high temperature over 310 °C and the photoinactive yellow phase with an orthorhombic lattice (δ-$CsPbI_3$) at lower temperatures [20,23], it is challenging to form the black phase at room temperature, except in the works of Snaith's group [20] and Hoffman *et al.* [17]. It is worth noting that nanoscale phases, such as quasi-two-dimensional nanoplates [24,25] and colloidal nanocrystal films [26–31], stabilize the cubic phase.

Alternatively, mixing the organic molecular cations with the inorganic alkali cations, forming double or triple mixed cations, has been reported to give rise to substantial enhancements of PV performance and phase stability for both single-junction and multijunction tandem solar cells [13,32–39]. Niu *et al.* [33] demonstrated that doping a small amount of Cs (~9%) into $MAPbI_3$ can stabilize the black perovskite

*ryongnam14@yahoo.com

structure, resulting in better thermal stability and device performance such as 18.1% PCE. When replacing 10% of FA with Cs in $FAPbI_3$, the PCE became as high as 19.0%, which was attributed to the strengthened interaction between FA and I due to a contraction of cubo-octahedral volume by Cs doping [34]. Furthermore, Cs-FA-MA triple-cation perovskites [37] and mixed-cation, mixed-halide perovskites (Cs-FA, I-Br) [36] have also been reported to exhibit better photostability and moisture stability and, moreover, effective reduction of the crystallization temperature during the annealing process. On the other hand, it was established that adding Rb can achieve more stable perovskite by better tuning the Goldschmidt tolerance factor [13,38,39]. Zhang *et al.* showed that 5% Rb in Rb-FA-MA triple-cation perovskite can provide the best film quality and a PCE of 20% on a 65-mm^2 device [38]. Very recently, it was reported that Rb-Cs-MA-FA quadruple-cation perovskites exhibit a band gap of 1.73 eV, negligible hysteresis, and steady-state efficiency as high as 17.4% and 26.4% in a tandem cell using a 23.9% *c*-Si cell, close to the current record for a single-junction Si cell of 26.6% [39].

These numerous experimental findings require systematically investigating the electronic structures, optical properties, and intrinsic material stability of $RbPbI_3$ and $CsPbI_3$ for better insight into materials engineering. To the best of our knowledge, however, computational works on these compounds are scarce when compared with the extensive studies on $MAPbI_3$ and $FAPbI_3$. Only one paper on the electronic band structures and dielectric properties of $RbPbI_3$ with both α and δ phases has been published [40], while there exist several works on $CsPbI_3$ [16,40–42] and $CsSnX_3$ [43–46].

In this work, we perform systematic first-principles calculations of the all-inorganic iodide perovskites $RbPbI_3$ and $CsPbI_3$ and their solid solutions $Rb_{1-x}Cs_xPbI_3$ by using the virtual-crystal approximation (VCA) method within density functional theory (DFT). Here, we assume that mixing Cs with Rb can stabilize the perovskite black phase in addition to the beneficial effect on band gap engineering based on the insight that $RbPbI_3$ does not undergo a phase transformation when temperature is increased [40]. First, we check the reliability of the exchange-correlation functional with calculations of lattice constants and band gaps of α-$CsPbI_3$ and $RbPbI_3$. While increasing the Cs content x from 0.0 to 1.0, we calculate the lattice constants, electronic band structures, and density of states (DOS) and optical properties with the inclusion of van der Waals (vdW) dispersion terms. We performed additional calculations of the DOS including the many-body interactions and spin-orbit coupling (SOC) effect with the GW+SOC method. Through these calculations, we will show the systematic variation tendency of material properties of inorganic solid solutions $Rb_{1-x}Cs_xPbI_3$ while varying the mixing ration x.

II. COMPUTATIONAL METHODS

Most of the calculations were carried out using the pseudopotential plane-wave method as implemented in the QUANTUM ESPRESSO package [47] (version 6.2). The ultrasoft pseudopotentials were generated using the ATOMIC code provided in the package, where the valence electronic configurations of atoms are Cs $6s^1$, Rb $5s^1$, I $5s^25p^5$, and Pb $6s^26p^2$. While increasing the Cs content x from 0.0 to 1.0 with a step of 0.1, we also generated pseudopotentials of virtual atoms $Rb_{1-x}Cs_x$ using the VCA method [48], as our previous studies for the hybrid mixed halide perovskites confirmed its efficiency and accuracy [49,50]. The plane-wave cutoff energy of 80 Ry and k-point mesh of $(8 \times 8 \times 8)$ for structural optimization guaranteed a total energy convergence of 1 meV per unit cell. We obtained the equilibrium lattice constants by calculating the total energies at different unit cell volumes and then fitting the obtained $E - V$ data into the Birch-Murnaghan equation of state [51]. All of the atomic positions were relaxed until the atomic forces were less than 0.02 eV $Å^{-1}$. For better calculations of the electronic and optical properties, we used a denser k-point mesh of $12 \times 12 \times 12$. The crystalline phases were supposed to be α phase with a $Pm\bar{3}m$ space group [23,52], as depicted in Fig. 1(a), since this phase is responsible for PSC performance and can be stabilized at room temperature [17,20].

The frequency-dependent dielectric constants, $\varepsilon(\omega) = \varepsilon_1(\omega) + i\varepsilon_2(\omega)$, were calculated within the density functional perturbation theory (DFPT) [53] as implemented in the

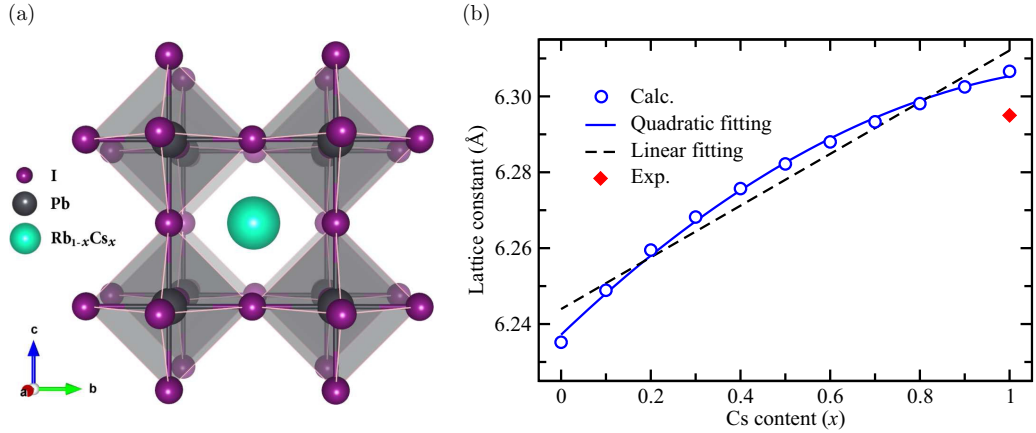

FIG. 1. (a) Polyhedral view of inorganic perovskite solid solution $Rb_{1-x}Cs_xPbI_3$ and (b) their lattice constants as a function of Cs content x. The fourth polynomial fitting, linear fitting, and experimental value for $CsPbI_3$ [52] are shown.

package. Then, the photoabsorption coefficients were obtained following [49,50,54]

$$\alpha(\omega) = \frac{2\omega}{c}\sqrt{\frac{\sqrt{\varepsilon_1^2(\omega)+\varepsilon_2^2(\omega)}-\varepsilon_1(\omega)}{2}}, \quad (1)$$

where c is the velocity of light. Within the Mott-Wannier model, the exciton binding energies were calculated as

$$E_b^{\mathrm{ex}} = \frac{m_e e^4}{2(4\pi\varepsilon_0)^2\hbar^2}\frac{m_r^*}{m_e}\frac{1}{\varepsilon_s^2} \approx 13.56\frac{m_r^*}{m_e}\frac{1}{\varepsilon_s^2}\ (\mathrm{eV}), \quad (2)$$

where m_r^* is the reduced effective mass evaluated by $1/m_r^* = 1/m_e^* + 1/m_h^*$ with the effective masses of electrons m_e^* and holes m_h^* and ε_s is the static dielectric constant.

To determine band gaps of $RbPbI_3$ and $CsPbI_3$ more precisely, we performed self-consistent GW calculations on top of Perdew-Burke-Ernzerhof (PBE) calculations (scGW@PBE) while considering of SOC effect, i.e., GW+SOC calculations, using the VASP code [55]. Self-consistency is important for calculations of material properties because it can remove the ambiguity produced by the starting-point dependence for one-shot GW calculation. To do this, ALGO parameter was set as scGW, where the eigenvalues and one-electron orbitals are updated [56]. After five iterations, the quasiparticle eigenvalues calculated by scGW@PBE were converged within 10^{-5} eV. For these calculations, we used a cutoff energy of 500 eV for the plane-wave basis set, a k-point mesh of $4\times4\times4$, and projector augmented-wave (PAW) potentials, for which valence electronic configurations are Cs $5s^25p^66s^1$, Rb $4s^24p^65s^1$, I $5s^25p^5$, and Pb $6s^26p^2$. Corresponding to the k-point mesh, the number of frequencies for the scGW calculations was set to 100, and the maximum angular quantum number l should be 4 to accurately describe the all-electron charge density on the plane-wave grid up to the radial quantum number of 4. Note that in the VASP code the maximum angular quantum number l is automatically set to 4 in GW calculations.

To determine the band gaps of $RbPbI_3$ and $CsPbI_3$ more precisely, we performed self-consistent GW calculations while considering the SOC effect, i.e., GW+SOC calculations, using the VASP code [55]. For these calculations, we used a cutoff energy of 500 eV for the plane-wave basis set, a k-point mesh of $4\times4\times4$, and PAW potentials, for which valence electronic configurations are Cs $5s^25p^66s^1$, Rb $4s^24p^65s^1$, I $5s^25p^5$, and Pb $6s^26p^2$. For the calculations of the response function, a smaller cutoff energy of 250 eV was used, together with the 80 Kohn-Sham (KS) states, where the first 34 were fully occupied and determined by the self-consistent field calculations.

III. RESULTS AND DISCUSSION

A. Assessment of the exchange-correlation functional

It is known that for inorganic compounds the exchange-correlation functionals within the local-density approximation overestimate the binding between atoms and underestimate the band gap by half of the experimental value, whereas those within the generalized gradient approximation (GGA) improve the accuracy with slight underestimations of both the binding and band gap. For example, the PBE functional [57], a typical GGA functional, gave the lattice constant of α-$CsPbI_3$ as 6.39 Å versus 6.29 Å in experiment [52] (relative error of 1.6%) and its band gap as 0.60 eV versus 1.73 eV in experiment [40]. It should be noted that, for the organic-inorganic hybrid halide perovskite $MAPbI_3$, the PBE functional can almost exactly reproduce the experimental band gap due to the fortuitous error cancellation between the underestimation by PBE and overestimation from ignoring the SOC effect [58], and the addition of vdW dispersion terms also slightly improves both the lattice constant and band gap [49,50,54]. Here, we tested the reliability of PBE, the PBE revised version for solids (PBEsol) [59], and PBE augmented with vdW interaction (PBE+vdW) [60] for lattice constant and band gap.

TABLE I. Lattice constant a and band gap E_g of inorganic perovskites $CsPbI_3$ and $RbPbI_3$, calculated using different exchange-correlation functionals. Experimental and previously calculated (Calc.) values are listed.

	This work			Previous work	
	PBE	PBEsol	PBE+vdW	Expt.	Calc.
$CsPbI_3$					
a (Å)	6.37	6.24	6.32	6.29[a]	6.26[b], 6.39[c], 6.18[d]
E_g (eV)	1.50	1.35	1.48	1.73[e]	0.51[b], 0.60[c], 1.30[d]
$RbPbI_3$					
a (Å)	6.31	6.18	6.23		6.39[c]
E_g (eV)	1.45	1.26	1.40		0.73[c]

[a]Reference [52].
[b]PBEsol for lattice constant and HSE06+SOC for band gap [16].
[c]PBE for lattice constant and HSE06+SOC for band gap [40].
[d]Full potential-linearized augmented plane wave (FP-LAPW) with the Wu-Cohen GGA functional [41].
[e]Reference [20].

Table I shows the calculated lattice constants and band gaps of α-$CsPbI_3$ and α-$RbPbI_3$ with the available experimental values and previously calculated values for comparison. The lattice constants were determined by the procedure described in Sec. II, i.e., by varying unit cell volumes evenly from $0.9V_0$ to $1.1V_0$ with the predetermined equilibrium volume V_0, calculating their total energies versus volume, and fitting the obtained $E-V$ data into the Birch-Murnaghan equation of states [51]. It is found from Table I that for $CsPbI_3$, PBE overestimates the experimental lattice constant with a relative error of 1.3%, and PBEsol underestimates it by −0.8%, in accordance with the previous calculations [16,40], whereas PBE+vdW gives the closest value, with a slight overestimation of 0.5%. This indicates that the addition of vdW interaction terms still improves the accuracy of calculations for all-inorganic halide perovskites as pointed out by Brgoch *et al.* [40]. It should be noted that for α-$RbPbI_3$ an experimental value is not available, and in Ref. [40] they strangely presented the same value for α-$CsPbI_3$, while in our calculation its lattice constant was calculated to be smaller by 0.06–0.09 Å than that of $CsPbI_3$ with a rational soundness due to the smaller ionic radius of Rb^+ compared with Cs^+.

Many previous DFT investigations [58,61] verified the important role of the relativistic effect of the heavy metallic elements in hybrid halide perovskites, which can be considered by the scalar relativistic effect approximately or by the

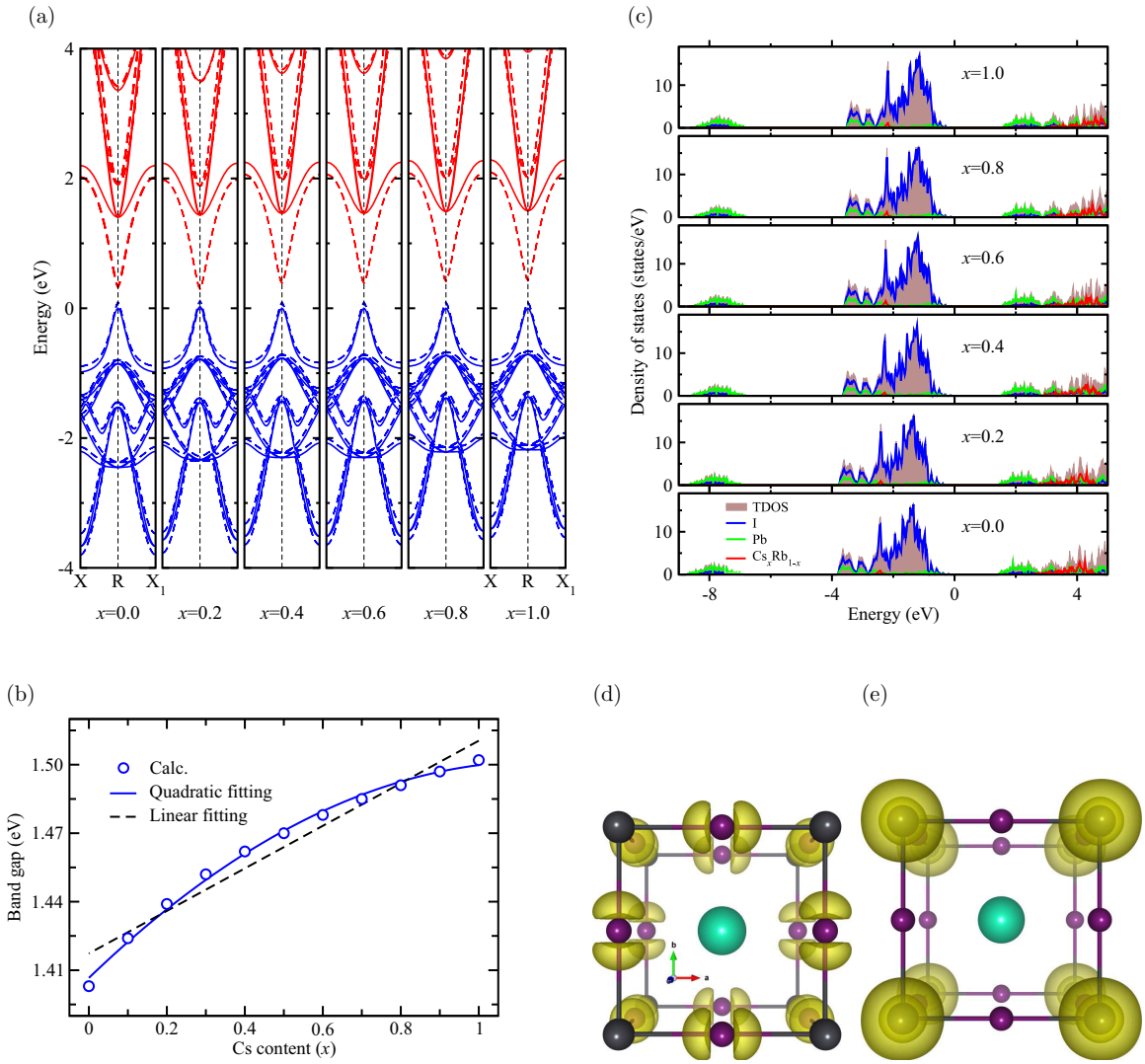

FIG. 2. Systematic change in electronic properties of inorganic iodide perovskite solid solutions $Rb_{1-x}Cs_xPbI_3$ while increasing the Cs content x, calculated with the PBE+vdW method. (a) Electronic band structures with (dashed line) and without (solid line) the SOC effect and (b) band gaps without the SOC effect as a function of Cs content x, with the fourth polynomial as well as linear fitting lines. (c) Total and atomic resolved electronic density of states, setting the valence band maximum (VBM) to zero. The charge density isosurface around (d) the VBM and (e) the conduction band minimum of $CsPbI_3$ at the value of 0.05 $|e|$ Å^{-3}.

SOC effect at higher levels. In order to check the importance of incorporating relativistic effects in the case of inorganic halide perovskites, we calculated electronic band structures with or without the SOC contribution, as shown in Fig. 2(a). Table I presents only band gaps calculated without SOC effects. Interestingly, for α-$CsPbI_3$, the calculated band gaps without SOC effects were in reasonable agreement with the experimental value of 1.73 eV [20], with slight underestimations of 0.25 eV (PBE), 0.38 eV (PBEsol), and 0.23 eV (PBE+vdW), again indicating the best agreement by the PBE+vdW functional. When including the SOC contribution, the deviation of the band gap from the experimental value became 1.20 eV, which is comparable to those in the case of hybrid halide perovskites. As clearly shown in Fig. 2(a), this is due to a split of the degenerate, unoccupied Pb_2^+ p orbitals and their downshift by the SOC effect. Such large deviations over 1 eV were also observed in previous computational studies [16,40], where Heyd-Scuseria-Ernzerhof in 2006 (HSE06)+SOC produced band gaps of 0.51–0.60 eV, resulting in deviations of 1.22–1.13 eV. Therefore, it became obvious that GGA and GGA+vdW (which is better without the SOC effect) are likely to describe the structural and electronic properties of inorganic halide perovskites as well as hybrid ones. It is worth noting that many-body interaction coupled with the SOC effect, i.e., GW+SOC, can give the most reliable band gaps, as we present later in this work. Henceforth, we progress using PBE+vdW without the SOC effect, aiming to find the variation tendency of the properties of their solid solutions $Rb_{1-x}Cs_xPbI_3$ while increasing x.

B. Lattice constants and electronic structures

Figure 1(b) shows the lattice constants of inorganic iodide perovskite solid solutions $Rb_{1-x}Cs_xPbI_3$ with the quadratic and linear fitting lines. It is shown that as the Cs content x increases, the lattice constant increases. Unlike

the hybrid mixed halide perovskite $MAPb(I_{1-x}Br_x)_3$ [49] or $MAPb(I_{1-x}Cl_x)_3$ [50], however, the lattice constants slightly deviate from Vegard's law; that is, their increasing tendency does not follow the linear function of Cs content x. That is why we tried to perform the quadratic fitting, resulting in a function of $a(x) = 6.237 + 0.113x - 0.045x^2$ (Å). It should be noted that the difference in lattice constants between $RbPbI_3$ and $CsPbI_3$ is not large (0.09 Å) compared with the case of mixed halide perovskites (0.3–0.7 Å). Since the deviation is not far from the linear fitting, we also tried to obtain the linear function as $a(x) = 6.244 + 0.068x$ (Å). For the sake of the reliability of VCA method, we also calculated the lattice constant and band gap of $Rb_{0.5}Cs0.5PbI_3$ using a $2 \times 2 \times 2$ supercell, resulting in 6.231 Å and 1.41 eV, which are in good agreement with the corresponding values of 6.282 Å and 1.47 eV using the VCA approach.

We show systematic change in electronic band structures of $Rb_{1-x}Cs_xPbI_3$ along the edge line of X-R-X_1 in reciprocal space (see Fig. S1 for the entire bands in the Supplemental Material [62]) while gradually increasing the Cs content x in Fig. 2(a), where the valence band maximum (VBM) is set to be zero. It was found that for all Cs contents, the PBE+vdW functional without a SOC contribution yields valence bands (VBs; blue solid lines) almost coincident with those incorporating the SOC effect (blue dashed lines), while the conduction bands (CBs) degenerated at the R point (red solid lines) compared with those split and downshifted by the SOC effect (red dashed lines). This resulted in the decrease of band gaps by as much as ~1.2 eV when including the SOC effect. It should be noted that the band gaps are characterized by a direct mode at the R point of reciprocal space, similar to the hybrid halide perovskites. This is one of the best advantages of a good solar absorber since the charge carriers such as electrons and holes can be directly generated by the absorption of photons without any energy loss by interacting with phonons.

Like lattice constants, the band gap E_g also increases going from $RbPbI_3$ to $CsPbI_3$, as shown in Fig. 2(b). Actually, when replacing the Cs^+ cation in α-$APbI_3$ by the Rb^+ cation with the smaller ionic radius, the interaction between Pb and I atoms within PbI_6 octahedra can be enhanced, resulting in the contraction of the crystalline lattice and, accordingly, an increase of the band gap. It is known that the variation tendency of band gaps while increasing the concentration of the composition of Cs in the hybrid mixed halide perovskites can be described by a quadratic function [49,50,63]. Interestingly, the band gap in the Rb-Cs inorganic halide perovskites also follows the quadratic function of Cs content x as $E_g(x) = 1.407 + 0.164x - 0.071x^2$ (eV), which can be reduced into the following equation:

$$E_g(x) = E_g(0) + [E_g(1) - E_g(0) - b]x + bx^2, \quad (3)$$

where $E_g(0) = 1.407$ eV is the band gap of $RbPbI_3$, $E_g(1) = 1.500$ eV is the band gap of $CsPbI_3$, and $b = -0.071$ eV is the bowing parameter, reflecting the fluctuation degree in the crystal field. The first notable difference from the hybrid mixed halide perovskites is the sign of the bowing parameter, which is negative in the case of inorganic mixed alkali iodide perovskites versus positive in the case of hybrid mixed halide perovskites. Since the bowing parameter is quite small, compositional disorder can be said to be low, and miscibility between $RbPbI_3$ and $CsPbI_3$ can be said to be good. Moreover, the decrease in band gap with increasing Rb content indicates an improvement of the light absorption property by mixing Cs with Rb.

In order to find the role of electrons of constituent atoms in the band structure, the electronic DOS was calculated and is presented in Fig. 2(c) (see Fig. S2 for partial DOS in the Supplemental Material [62]). We see that the upper VBs and lower CBs responsible for the transport of charge carriers (electrons and holes) come from the overlap of I $5p$/Pb $6s$ states and the Pb $6p$ state, respectively. This is rational because the Pb_2^+ cation has a filled $6s$ state and an empty $6p$ state, while the I^- anion has a completely filled $5p$ state. The $5/6s$ atomic orbitals of Rb/Cs are found far below and above the VBM and conduction band minimum (CBM), indicating that the $(Rb_{1-x}Cs_x)^+$ ($x = [0, 1]$) cation is electronically inert [16]. Similar observations were made for the hybrid mixed halide perovskites [49,50]. Notably, it was observed that the VBM is characterized by the I $5p$ state, and the CBM is characterized by the Pb $6s$ state, as shown in Figs. 2(d) and 2(e) (see Fig. S3 for those of $RbPbI_3$ in the Supplemental Material [62]), whereas in the case of hybrid halide perovskites the VBM is formed from the overlap of I $5p$ and Pb $6s$ states and the CBM is formed from the Pb $6p$ state.

As we discussed above, the band gaps were remarkably underestimated by including the SOC effect due to the downshift of the CBM composed of Pb atomic orbitals. This can be cured by adding the effect of many-body interactions within the GW approximation, which overestimates the band gap (see Fig. S4 in the Supplemental Material [62]). We treated only the pure $RbPbI_3$ and $CsPbI_3$ compounds with the optimized structures by using the PBE+vdW functional and considering the SOC effect to see the improvement of the band gap calculation with the GW+SOC method. Given that the number of valence electrons in the unit cell is 34, which can be determined from the valence electronic configurations of PAW potentials (see Sec. II) for the constituent atoms, the occupied Kohn-Sham (KS) states of 17 were considered in this calculation. Figure 3 shows their DOSs calculated by the GW+SOC method, together with the total DOS (TDOS) calculated using the PBE+vdW functional for a comparison. It was found that for $CsPbI_3$ the DFT VBM and CBM are pushed up by 0.91 and 1.06 eV, respectively, resulting in a total upshift of 0.15 eV of the DFT band gap (1.48 eV) and thus an improved band gap of 1.65 eV, with only a deviation of 0.08 eV from the experimental value of 1.73 eV. For the case of $RbPbI_3$, the upshifts of VBM and CBM are 1.05 and 1.12 eV, respectively, which gives a total upshift of the DFT band gap (1.40 eV) of 0.07 eV.

C. Optical properties and charge carrier transport

The photoabsorption coefficient is a major optical property that determines the capability of the light absorber for harvesting solar energy. This can be obtained using Eq. (1) with the calculated macroscopic dielectric constants as a function of frequency. Our previous calculations for the hybrid halide perovskites [50] found that the DFPT approach, considering the effect of atomic displacements, can yield dielectric constants

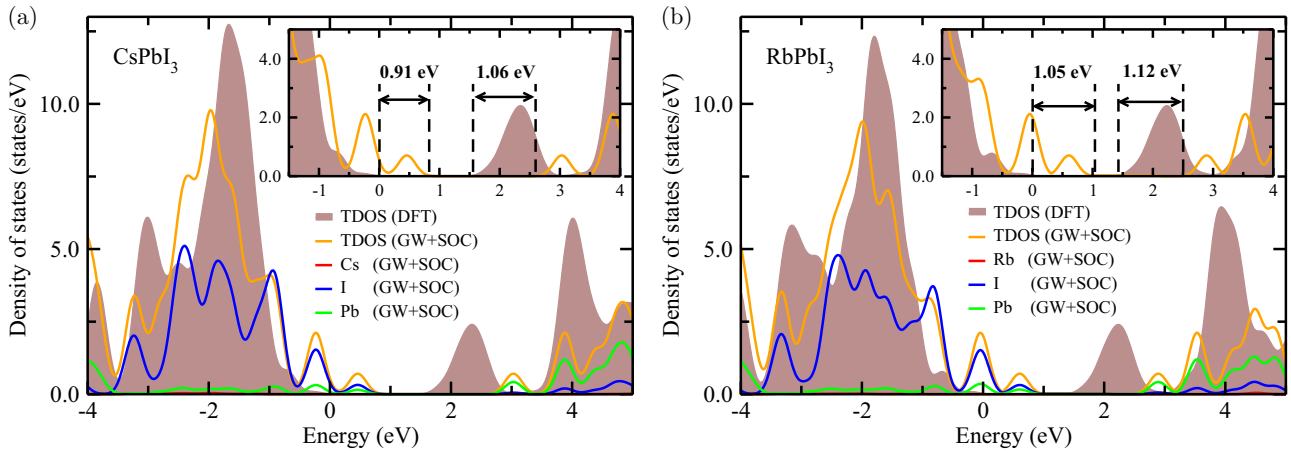

FIG. 3. Total and atomic resolved electronic density of states (DOS) of (a) $CsPbI_3$ and (b) $RbPbI_3$, calculated by using the GW+SOC method. For comparison, TDOS calculated using the PBE+vdW functional is also shown. Insets present the shifts of the VBM and CBM explicitly.

almost identical to those of the Bethe-Salpeter approach including the excitonic and many-body effects. In this work, therefore, we performed the DFPT calculations of the macroscopic dielectric constants with their real and imaginary parts (see Fig. S5 in the Supplemental Material [62]). In Fig. 4(a), we plot the photoabsorption coefficients as a function of photon energy (frequency) while increasing the Cs content x. For higher Cs contents, since the band gap gradually increases

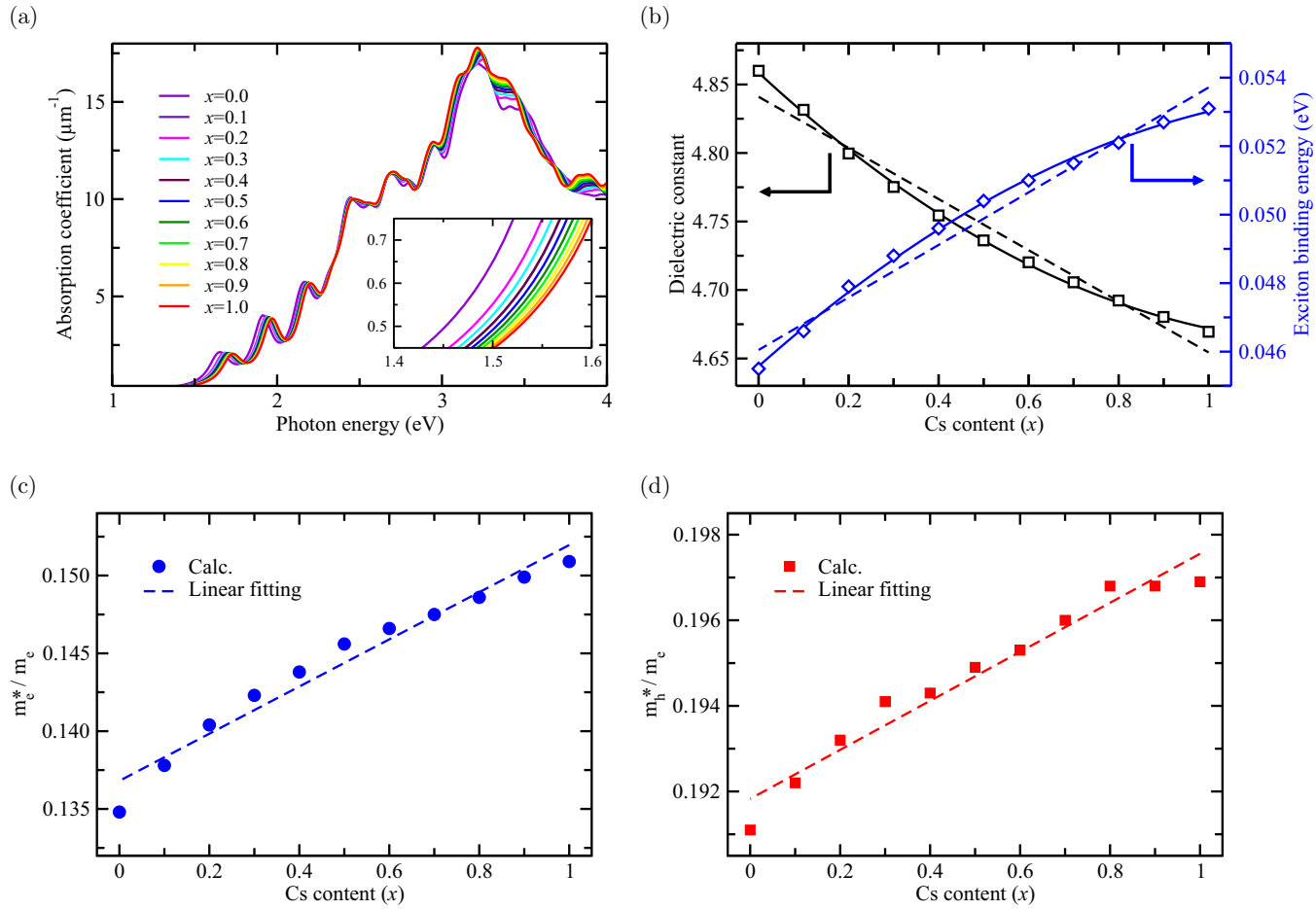

FIG. 4. (a) Photoabsorption coefficients, (b) static dielectric constants, and exciton binding energies and (c) and (d) effective masses of electrons and holes in the inorganic iodide perovskite solid solutions $Rb_{1-x}Cs_xPbI_3$ while increasing the Cs content x from 0 to 1, calculated with the PBE+vdW method.

as discussed above, the absorption onsets are shifted, at a slow pace, to the ultraviolet region in the solar spectrum, indicating a harshening of photoabsorption capability. The maximum photoabsorption coefficients were found to be slightly lower, with a value $\sim 17\,\mu\mathrm{m}^{-1}$, at the position of ~ 3.25 eV than those ($\sim 22\,\mu\mathrm{m}^{-1}$) of the hybrid halide perovskites [49,50].

The static dielectric constants were extracted from the frequency-dependent macroscopic dielectric functions at the zero photon energy to be used for the calculation of the exciton binding energy. As shown in Fig. 4(b), they decrease in accordance with the quadratic function of Cs content x as $\varepsilon_s(x) = 4.859 - 0.304x + 0.117x^2$, which is different from the linear function in the case of the hybrid halide perovskites [50]. We also tried to fit them into the linear function, yielding $\varepsilon_s(x) = 4.841 - 0.187x$. For pure $CsPbI_3$ ($RbPbI_3$), our calculated value of 4.7 (4.9) is in reasonable agreement with the previous theoretical value of 5.3 (4.8) calculated with the PBE+SOC approach [40]. On the other hand, these values are comparable with those of the hybrid halide perovskite, e.g., 5.6 for $MAPbI_3$ [50].

In order to see how the charge carriers such as electrons and holes behave after being generated by absorbing photons, we calculated effective masses of electrons (m_e^*) and holes (m_h^*) and exciton binding energy, which are useful for a qualitative estimation of charge carrier mobility. The effective masses of electrons and holes were calculated around the CBM and VBM at the R point using the refined energy band structure within the parabolic approximation. As shown in Figs. 4(c) and 4(d), they slightly increase along the linear functions of Cs content as $m_e^*(x) = (0.137 + 0.015x)m_e$ and $m_h^*(x) = (0.192 + 0.006x)m_e$, respectively, indicating an enhancement of charge carrier mobilities upon the Rb addition to $CsPbI_3$. For pristine $CsPbI_3$, the calculated values of $m_e^* = 0.15m_e$ and $m_h^* = 0.20m_e$ are comparable to the previous theoretical values of $m_e^* = 0.22m_e$ and $m_h^* = 0.19m_e$ with the modified Becke-Johnson approach [42] and $m_h^* = 0.16m_e$ with the HSE06+SOC approach [16]. Moreover, these values are slightly lower than those of $MAPbI_3$ obtained with the same level of theory [50] ($m_e^* = 0.20m_e$ and $m_h^* = 0.23m_e$), indicating lighter carriers in $CsPbI_3$, which might be very promising for the efficiency of solar cells.

Finally, we consider the exciton binding energies E_b calculated by Eq. (2) using the static dielectric constants and charge carrier effective masses. Since the exciton binding energy is a direct estimation of the electrostatic attraction between electrons and holes, its smaller value indicates freelike charge carriers. As shown in Fig. 4(b), they increase according to the quadratic function of $E_b(x) = 0.046 + 0.012x - 0.004x^2$ (eV) with increasing Cs content due to the decrease of the static dielectric constants and increase of the charge carrier effective masses. This again indicates an enhancement of solar cell performance upon the Rb addition to $CsPbI_3$. Furthermore, these are comparable to $MAPbI_3$ and the inorganic thin-film semiconductors, indicating that the charge carriers in the all-inorganic alkali iodide perovskite, generated by photoabsorption, can behave as if they are free.

IV. CONCLUSIONS

Using the virtual-crystal approximation method, we have systematically investigated the electronic and optical properties of the inorganic alkali iodide perovskite solid solutions $Rb_{1-x}Cs_xPbI_3$. Through the assessment of the exchange-correlation functional, the PBE+vdW approach was selected to be the most reliable for both the lattice constant and band gap. When increasing the Cs content x from 0.0 to 1.0, the lattice constants and band gaps increase following the quadratic functions of $a(x) = 6.237 + 0.113x - 0.045x^2$ (Å) and $E_g(x) = 1.407 + 0.164x - 0.071x^2$ (eV), respectively, indicating a redshift of absorption onset in $RbPbI_3$ compared to $CsPbI_3$. It was found that the upper VBs and lower CBs come from the overlap of I $5p$/Pb $6s$ states and the Pb $6p$ states. The GW+SOC approach was confirmed to improve the band gap calculation, giving a band gap of 1.65 eV for $CsPbI_3$, in good agreement with the experimental value of 1.73 eV, although the PBE+SOC approach gave the worst value. The photoabsorption coefficients were obtained using the real and imaginary parts of macroscopic dielectric functions calculated by the DFPT method. With increasing Cs content, the static dielectric constants decrease following the quadratic function of $\varepsilon_s(x) = 4.859 - 0.304x + 0.117x^2$, and accordingly, the exciton binding energies increase according to the quadratic function of $E_b(x) = 0.046 + 0.012x - 0.004x^2$ (eV). Together with the linear decreases of electron and hole effective masses, these indicate a possible enhancement of solar cell performance upon the Rb addition to $CsPbI_3$.

ACKNOWLEDGMENTS

This work was supported partially by the State Committee of Science and Technology, Democratic People's Republic of Korea, under the state research project "Design of Innovative Functional Materials for Energy and Environmental Application" (No. 2016-20). The calculations were carried out on the HP Blade System C7000 (HP BL460c) that is owned by the Faculty of Materials Science, Kim Il Sung University.

[1] M. Liu, M. B. Johnston, and H. J. Snaith, Efficient planar heterojunction perovskite solar cells by vapor deposition, Nature (London) **501**, 395 (2013).

[2] J. Burschka, N. Pellet, S. J. Moon, R. Humphry-Baker, P. Gao, M. K. Nazeeruddin, and M. Grätzel, Sequential deposition as a route to high-performance perovskite-sensitized solar cells, Nature (London) **499**, 316 (2013).

[3] W. S. Yang, B. W. Park, E. H. Jung, N. J. Jeon, Y. C. Kim, D. U. Lee, S. S. Shin, J. Seo, E. K. Kim, J. H. Noh *et al.*, Iodide management in formamidinium-lead-halide-based perovskite layers for efficient solar cells, Science **356**, 1376 (2017).

[4] A. M. Ganose, C. N. Savory, and D. O. Scanlon, Beyond methylammonium lead iodide: Prospects for the emergent field of ns^2 containing solar absorbers, Chem. Commun. **53**, 20 (2017).

[5] T. Baikie, Y. N. Fang, J. M. Kadro, M. Schreyer, F. X. Wei, S. G. Mhaisalkar, M. Grätzel, and T. J. White, Synthesis and

crystal chemistry of the hybrid perovskite $(CH_3NH_3)PbI_3$ for solid-state sensitised solar cell applications, J. Mater. Chem. A **1**, 5628 (2013).

[6] V. D'Innocenzo, G. Grancini, M. J. P. Alcocer, A. R. S. Kandada, S. D. Stranks, M. M. Lee, G. Lanzani, H. J. Snaith, and A. Petrozza, Excitons versus free charges in organo-lead tri-halide perovskites, Nat. Commun. **5**, 3486 (2014).

[7] Y. Shao, Z. Xiao, C. Bi, Y. Yuan, and J. Huang, Origin and elimination of photocurrent hysteresis by fullerene passivation in $CH_3NH_3PbI_3$ planar heterojunction solar cells, Nat. Commun. **5**, 5784 (2014).

[8] A. Walsh, D. O. Scanlon, S. Chen, X. G. Gong, and S.-H. Wei, Self-regulation mechanism for charged point defects in hybrid halide perovskites, Angew. Chem. Int., Ed. **54**, 1791 (2015).

[9] B. Li, Y. Li, C. Zheng, D. Gao, and W. Huang, Advancements in the stability of perovskite solar cells: Degradation mechanisms and improvement approaches, RSC Adv. **6**, 38079 (2016).

[10] T. A. Berhe, W.-N. Su, C.-H. Chen, C.-J. Pan, J.-H. Cheng, H.-M. Chen, M.-C. Tsai, L.-Y. Chen, A. A. Dubaleb, and B.-J. Hwang, Organometal halide perovskite solar cells: Degradation and stability, Energy Environ. Sci. **9**, 323 (2016).

[11] X. Li, F. Cao, D. Yu, J. Chen, Z. Sun, Y. Shen, Y. Zhu, L. Wang, Y. Wei, Y. Wu *et al.*, All inorganic halide perovskites nanosystem: Synthesis, structural features, optical properties and optoelectronic applications, Small **13**, 1603996 (2017).

[12] A. Walsh, Principles of chemical bonding and band gap engineering in hybrid organic-inorganic halide perovskites, J. Phys. Chem. C **119**, 5755 (2015).

[13] M. Saliba, T. Matsui, K. Domanski, J.-Y. Seo, A. Ummadisingu, S. M. Zakeeruddin, J.-P. Correa-Baena, W. R. Tress, A. Abate, A. Hagfeldt *et al.*, Incorporation of rubidium cations into perovskite solar cells improves photovoltaic performance, Science **354**, 206 (2016).

[14] V. M. Goldschmidt, Die gesetze der krystallochemie, Naturwissenschaften **14**, 477 (1926).

[15] R. D. Shannon, Revised effective ionic-radii and systematic studies of interatomic distances in halides and chalcogenides, Acta Crystallogr., Sect. A **32**, 751 (1976).

[16] C. H. Hendon, R. X. Yang, L. A. Burton, and A. Walsh, Assessment of polyanion (BF_4^- and PF_6^-) substitutions in hybrid halide perovskites, J. Mater. Chem. A **3**, 9067 (2015).

[17] J. B. Hoffman, A. L. Schleper, and P. V. Kamat, Transformation of sintered $CsPbBr_3$ nanocrystals to cubic $CsPbI_3$ and gradient $CsPbBr_xI_{3-x}$ through halide exchange, J. Am. Chem. Soc. **138**, 8603 (2016).

[18] M. Kulbak, D. Cahen, and G. Hodes, How important is the organic part of lead halide perovskite photovoltaic cells? Efficient $CsPbBr_3$ cells, J. Phys. Chem. Lett. **6**, 2452 (2015).

[19] A. Kovalsky, L. Wang, G. T. Marek, C. Burda, and J. S. Dyck, Thermal conductivity of $CH_3NH_3PbI_3$ and $CsPbI_3$: Measuring the effect of the methylammonium ion on phonon scattering, J. Phys. Chem. C **121**, 3228 (2017).

[20] G. E. Eperon, G. M. Paternó, R. J. Sutton, A. Zampetti, A. A. Haghighirad, F. Cacialli, and H. J. Snaith, Inorganic caesium lead iodide perovskite solar cells, J. Mater. Chem. A **3**, 19688 (2015).

[21] W. Ahmad, J. Khan, G. Niu, and J. Tang, Inorganic $CsPbI_3$ perovskite-based solar cells: A choice for a tandem device, Sol. RRL **1**, 1700048 (2017).

[22] K. Heidrich, W. Schafer, M. Schreiber, J. Sochtig, G. Trendel, J. Treusch, T. Grandke, and H. J. Stolz, Electronic structure, photoemission spectra, and vacuum-ultraviolet optical spectra of $CsPbCl_3$ and $CsPbBr_3$, Phys. Rev. B **24**, 5642 (1981).

[23] C. K. Moller, Crystal structure and photoconductivity of caesium plumbohalides, Nature (London) **182**, 1436 (1958).

[24] Y. Bekenstein, B. A. Koscher, S. W. Eaton, P. Yang, and A. P. Alivisatos, Highly luminescent colloidal nanoplates of perovskite cesium lead halide and their oriented assemblies, J. Am. Chem. Soc. **137**, 16008 (2015).

[25] A. Swarnkar, A. R. Marshall, E. M. Sanehira, B. D. Chernomordik, D. T. Moore, J. A. Christians, T. Chakrabarti, and J. M. Luther, Quantum dot-induced phase stabilization of α-$CsPbI_3$ perovskite for high-efficiency photovoltaics, Science **354**, 92 (2016).

[26] N. J. L. K. Davis, F. J. de la Peña, M. Tabachnyk, J. M. Richter, R. D. Lamboll, E. P. Booker, F. W. R. Rivarola, J. T. Griffiths, C. Ducati, S. M. Menke *et al.*, Photon reabsorption in mixed $CsPbCl_3$:$CsPbI_3$ perovskite nanocrystal films for light-emitting diodes, J. Phys. Chem. C **121**, 3790 (2017).

[27] Q. A. Akkerman, V. D'Innocenzo, S. Accornero, A. Scarpellini, A. Petrozza, M. Prato, and L. Manna, Tuning the optical properties of cesium lead halide perovskite nanocrystals by anion exchange reactions, J. Am. Chem. Soc. **137**, 10276 (2015).

[28] G. Nedelcu, L. Protesescu, S. Yakunin, M. I. Bodnarchuk, M. J. Grotevent, and M. V. Kovalenko, Fast anion-exchange in highly luminescent nanocrystals of cesium lead halide perovskites ($CsPbX_3$, X = Cl, Br, I), Nano Lett. **15**, 5635 (2015).

[29] L. Gomez, C. de Weerd, J. L. Huesob, and T. Gregorkiewicza, Color-stable water-dispersed cesium lead halide perovskite nanocrystals, Nanoscale **9**, 631 (2017).

[30] Q. Liu, Y. Wang, N. Sui, Y. Wang, X. Chi, Q. Wang, Y. Chen, W. Ji, L. Zou, and H. Zhang, Exciton relaxation dynamics in photo-excited $CsPbI_3$ perovskite nanocrystals, Sci. Rep. **6**, 29442 (2016).

[31] L. Protesescu, S. Yakunin, M. I. Bodnarchuk, F. Krieg, R. Caputo, C. H. Hendon, R. X. Yang, A. Walsh, and M. V. Kovalenko, Nanocrystals of cesium lead halide perovskites ($CsPbX_3$, X = Cl, Br, and I): Novel optoelectronic materials showing bright emission with wide color gamut, Nano Lett. **15**, 3692 (2015).

[32] Z. Li, M. Yang, J.-S. Park, S.-H. Wei, J. J. Berry, and K. Zhu, Stabilizing perovskite structures by tuning tolerance factor: Formation of formamidinium and cesium lead iodide solid-state alloys, Chem. Mater. **28**, 284 (2016).

[33] G. Niu, W. Li, J. Li, X. Liang, and L. Wang, Enhancement of thermal stability for perovskite solar cells through cesium doping, RSC Adv. **7**, 17473 (2017).

[34] J.-W. Lee, D.-H. Kim, H.-S. Kim, S.-W. Seo, S. M. Cho, and N.-G. Park, Formamidinium and cesium hybridization for photo- and moisture-stable perovskite solar cell, Adv. Energy Mater. **5**, 1501310 (2015).

[35] D. P. McMeekin, G. Sadoughi, W. Rehman, G. E. Eperon, M. Saliba, M. T. Horantner, A. Haghighirad, N. Sakai, L. Korte, B. Rech *et al.*, A mixed-cation lead mixed-halide perovskite absorber for tandem solar cells, Science **351**, 151 (2016).

[36] W. Rehman, D. P. McMeekin, J. B. Patel, R. L. Milot, M. B. Johnston, H. J. Snaith, and L. M. Herz, Photovoltaic mixed-cation lead mixed-halide perovskites: Links between

crystallinity, photo-stability and electronic properties, Energy Environ. Sci. **10**, 361 (2017).

[37] M. Saliba, T. Matsui, J.-Y. Seo, K. Domanski, J.-P. Correa-Baena, M. K. Nazeeruddin, S. M. Zakeeruddin, W. Tress, A. Abate, A. Hagfeldtd *et al.*, Cesium-containing triple cation perovskite solar cells: Improved stability, reproducibility and high efficiency, Energy Environ. Sci. **9**, 1989 (2016).

[38] M. Zhang, J. S. Yun, Q. Ma, J. Zheng, C. F. J. Lau, X. Deng, J. Kim, D. Kim, J. Seidel, M. A. Green *et al.*, High-efficiency rubidium-incorporated perovskite solar cells by gas quenching, ACS Energy Lett. **2**, 438 (2017).

[39] T. Duong, Y. L. Wu, H. Shen, J. Peng, X. Fu, D. Jacobs, E.-C. Wang, T. C. Kho, K. C. Fong, M. Stocks *et al.*, Rubidium multication perovskite with optimized bandgap for perovskite-silicon tandem with over 26% efficiency, Adv. Energy Mater. **7**, 1700228 (2017).

[40] J. Brgoch, A. J. Lehner, M. Chabinyc, and R. Seshadri, Ab initio calculations of band gaps and absolute band positions of polymorphs of $RbPbI_3$ and $CsPbI_3$: Implications for main-group halide perovskite photovoltaics, J. Phys. Chem. C **118**, 27721 (2014).

[41] G. Murtaza and I. Ahmad, First principle study of the structural and optoelectronic properties of cubic perovskites $CsPbM_3$ (M = Cl, Br, I), Phys. B (Amsterdam, Neth.) **406**, 3222 (2011).

[42] M. Afsari, A. Boochani, and M. Hantezadeh, Electronic, optical and elastic properties of cubic perovskite $CsPbI_3$: Using first principles study, Optik **127**, 11433 (2016).

[43] R. X. Yang, J. M. Skelton, E. L. da Silva, J. M. Frost, and A. Walsh, Spontaneous octahedral tilting in the cubic inorganic caesium halide perovskites $CsSnX_3$ and $CsPbX_3$ (X = F, Cl, Br, I), J. Phys. Chem. Lett. **8**, 4720 (2017).

[44] G. Song, B. Gao, G. Li, and J. Zhang, First-principles study on the electric structure and ferroelectricity in epitaxial $CsSnI_3$ films, RSC Adv. **7**, 41077 (2017).

[45] E. L. da Silva, J. M. Skelton, S. C. Parker, and A. Walsh, Phase stability and transformations in the halide perovskite $CsSnI_3$, Phys. Rev. B **91**, 144107 (2015).

[46] L. Y. Huang and W. R. L. Lambrecht, Electronic band structure, phonons, and exciton binding energies of halide perovskites $CsSnCl_3$, $CsSnBr_3$, and $CsSnI_3$, Phys. Rev. B **88**, 165203 (2013).

[47] P. Giannozzi, S. Baroni, N. Bonini, M. Calandra, R. Car *et al.*, Quantum espresso: A modular and open-source software project for quantum simulations of materials, J. Phys.: Condens. Matter **21**, 395502 (2009).

[48] C.-J. Yu and H. Emmerich, An efficient virtual crystal approximation that can be used to treat heterovalent atoms, applied to $(1-x)BiScO_3-xPbTiO_3$, J. Phys.: Condens. Matter **19**, 306203 (2007).

[49] U.-G. Jong, C.-J. Yu, J.-S. Ri, N.-H. Kim, and G.-C. Ri, Influence of halide composition on the structural, electronic, and optical properties of mixed $CH_3NH_3Pb(I_{1-x}Br_x)_3$ perovskites calculated using the virtual crystal approximation method, Phys. Rev. B **94**, 125139 (2016).

[50] U.-G. Jong, C.-J. Yu, Y.-M. Jang, G.-C. Ri, S.-N. Hong, and Y.-H. Pae, Revealing the stability and efficiency enhancement in mixed halide perovskites $MAPb(I_{1-x}Cl_x)_3$ with ab initio calculations, J. Power Sources **350**, 65 (2017).

[51] F. Birch, Finite elastic strain of cubic crystal, Phys. Rev. **71**, 809 (1947).

[52] D. M. Trots and S. V. Myagkota, High-temperature structural evolution of caesium and rubidium triiodoplumbates, J. Phys. Chem. Solids **69**, 2520 (2008).

[53] S. Sharma, J. K. Dewhurst, and C. Ambrosch-Draxl, Linear and second-order optical response of III-V monolayer superlattices, Phys. Rev. B **67**, 165332 (2003).

[54] C.-J. Yu, U.-G. Jong, M.-H. Ri, G.-C. Ri, and Y.-H. Pae, Electronic structure and photoabsorption property of pseudocubic perovskites $CH_3NH_3PbX_3$ (X = I, Br) including van der Waals interaction, J. Mater. Sci. **51**, 9849 (2016).

[55] G. Kresse and J. Furthmüller, Effciency of ab-initio total energy calculations for metals and semiconductors using a plane-wave basis set, Comput. Mater. Sci. **6**, 15 (1996).

[56] M. Shishkin and G. Kresse, Self-consistent GW calculations for semiconductors and insulators, Phys. Rev. B **75**, 235102 (2007).

[57] J. P. Perdew, K. Burke, and M. Ernzerhof, Generalized Gradient Approximation Made Simple, Phys. Rev. Lett. **77**, 3865 (1996).

[58] J. Even, L. Pedesseau, J.-M. Jancu, and C. Katan, Importance of spin-orbit coupling in hybrid organic/inorganic perovskites for photovoltaic applications, J. Phys. Chem. Lett. **4**, 2999 (2013).

[59] J. P. Perdew, A. Ruzsinszky, G. I. Csonka, O. A. Vydrov, G. E. Scuseria, L. A. Constantin, X. Zhou, and K. Burke, Restoring the Density Gradient Expansion for Exchange in Solids and Surfaces, Phys. Rev. Lett. **100**, 136406 (2008).

[60] K. Lee, E. D. Murray, L. Kong, B. I. Lundqvist, and D. C. Langreth, High-accuracy van der Waals density functional, Phys. Rev. B **82**, 081101(R) (2010).

[61] P. Umari, E. Mosconi, and F. D. Angelis, Relativistic GW calculations on $CH_3NH_3PbI_3$ and $CH_3NH_3SnI_3$ perovskites for solar cell applications, Sci. Rep. **4**, 4467 (2014).

[62] See Supplemental Material at http://link.aps.org/supplemental/10.1103/PhysRevB.98.125116 for electronic band structures of $CsPbI_3$, $RbPbI_3$, and $Rb_{0.4}Cs_{0.6}PbI_3$ along the complete line in the Brillouin zone, their partial density of states, isosurface plots of the valence band maximum and conduction band minimum of $RbPbI_3$, and real and imaginary parts of dielectric constants with increasing Cs content x.

[63] L. Atourki, E. Vega, B. Marì, M. Mollarb, H. A. Ahsainec, K. Bouabida, and A. Ihlal, Role of the chemical substitution on the structural and luminescence properties of the mixed halide perovskite thin $MAPbI_{3-x}Br_x$ $(0 < x < 1)$ films, Appl. Surf. Sci. **371**, 112 (2016).